JOURNAL OF MATERIALS SCIENCE 29 (1994) 5839–5846

# Thermal degradation mechanisms of Nicalon fibre: a thermodynamic simulation

C. VAHLAS
*Laboratoire Marcel Mathieu, CNRS-UPPA, Centre Hélioparc, 2 avenue du Président P. Angot, 64000 Pau, France*

P. ROCABOIS, C. BERNARD
*Laboratoire de Thermodynamique et Physicochimie Métallurgiques, URA 29 CNRS-INPG, Domaine Universitaire, BP 75, 38402 Saint Martin d'Hères, France*

Thermodynamic calculations for the thermal degradation of the Nicalon fibre in inert gas flow at atmospheric pressure have been performed, based on minimization of the Gibbs energy of the Si–C–O–H chemical system. The calculations are based on a critically selected thermodynamic database of the participating compounds. The results are presented by means of diagrams illustrating the quantities of condensed and gaseous species obtained as a function of treatment temperature. These are compared with recently reported TEM studies of as-received and heat-treated material, which illustrate the sequential morphologies of its structure and nanotexture as a function of treatment temperature. The main step of the observed degradation mechanism is successfully simulated in terms of the temperature, the oxygen content and the weight loss of the material. An endogenous oxidation mechanism is proposed for degradation of the fibre.

## 1. Introduction

A model for the structure and nanotexture together with mechanisms of the thermal degradation of ceramic-grade Nicalon® fibre NL-202 (Nippon Carbon, Yokohama, Japan) were recently proposed, based on transmission electron microscopy studies [1]. In accordance with other investigations [2–5], the fibre was found to be a microcomposite containing SiC grains, a free carbon network and an intergranular phase (solid solution) whose average composition was proposed [1] to be $SiO_{1.15}C_{0.85}$. The global composition by weight of the fibre was determined as 55% β-SiC crystals, 40% $SiO_{1.15}C_{0.85}$ intergranular phase and 5% free carbon. 0.2 wt %(3.7 at %) hydrogen was also evidenced as a residue of the precursor material.

The presence of an external silica layer which covers the desized fibre has also been reported [3] and attributed to the manufacturing process; the average composition of the non-stoichiometric phase was proposed to be $SiO_{1.09}C_{0.45}$ and the overall composition by weight was determined as 57% β-SiC, 31% $SiO_{1.09}C_{0.45}$ and 12% C. The difference in composition between the above-mentioned values concerning the fibre and the $SiO_xC_y$ phase may be due to the assumptions made (the amounts $x + y$ in [1] and $x + 2y$ in [3] were taken equal to 2), to the precision of the analytical methods adopted and to the low reproducibility of the industrial fibre itself.

Thermal treatments of this and previous versions of the Nicalon fibre in inert atmospheres have also been reported in the literature [1, 2, 6–11]. The corresponding results [1] led to the subsequent determination of its structure and nanotexture. Two major overlapping steps were thus recognized, following the temperature of treatment. In the first step, which is still apparent at 1523 K, the major phenomenon occurring is modification of the structure of free carbon. This was attributed to the release of hydrogen from the carbon network, which is completed at the above temperature, as was also evidenced by multiple Knudsen cell mass spectrometry measurements [12]. No other chemical modification was reported in this step. In the second step, which is completed by 1773 K, a drastic change in the fibre nanotexture was observed, due to the release of the contained oxygen in the form of carbon and silicon monoxides; this leads to destruction of the intergranular phase, to a strong degradation of the free carbon, and to a widening of the β-SiC crystals. A mechanism was proposed to explain this behaviour, based on the reaction of the released oxygen with the free carbon as well as with the carbon and silicon of the $SiO_{1.15}C_{0.85}$ phase to give gaseous CO and SiO, and SiC, following the overall scheme

$$0.7\ SiO_{1.15}C_{0.85(s)} + 0.42\ C_{(s)} \rightarrow 0.24\ SiO_{(g)} + 0.56\ CO_{(g)} + 0.46\ SiC_{(s)} \quad (1)$$

An intermediate third step was also evidenced at 1673 K with the occurrence of a skin-and-core effect, indicating that for the heating profile adopted, the external part of the fibre has, in contrast to the internal part, already reached a structure and composition corresponding to its degraded state.

0022–2461 

In the light of these recent experimental contributions in understanding Nicalon fibre, a thermodynamic study of the conditions of its thermal degradation allows a check of the proposed reactions with the aim of defining the relationship between the behaviour of the material under different operating conditions and the corresponding degradation or reaction mechanisms. On this basis, surface and interface kinetic and diffusion studies of the thermal and/or chemical degradation mechanisms, applied to the core (condensed phases) and the skin (condensed and gas phases) of the fibre, can build up a complete model aiming at *a priori* establishment of the operating limits of this material and prediction of the behaviour of other oxygen-containing silicon carbide-based ceramic fibres.

Studies of particular reactions which are presumed to occur in the Si–C–O system under operating conditions close to the conditions of the heat treatment of Nicalon fibre have already been reported in the literature [13–16]. Additionally, the approach consisting of taking into account all the compounds which can potentially participate in the corresponding chemical system and to minimize the total Gibbs energy by means of suitable computer software has also been used by Greil [17], who considered the fibre as an SiC, $SiO_2$ and C containing material, by Benson *et al.* [18] who simulated the interfacial behaviour of Nicalon fibre-containing composites, and by Jacobson *et al.* [19] who studied the thermodynamics of the SiC–$SiO_2$ and equimolar SiC–$SiO_2$–C interactions.

In this paper the results of thermodynamic calculations concerning the heat treatment of NL-202 Nicalon fibre in an inert gas flow at atmospheric pressure are reported. Firstly the principle and the different types of calculation as a function of the experimental situation to be simulated are discussed, together with a critical selection of thermodynamic data for the species considered. The results of calculations are presented by means of yield diagrams indicating the number of moles obtained at equilibrium for the condensed and gaseous species as a function of temperature. The validity of the approach adopted is discussed and the results obtained are compared with available experimental information.

## 2. Thermodynamics

The calculations were based on the minimization of the Gibbs energy $G$ of the chemical system generated from combinations of the elements Si–C–O–H–Ar. Thirty-one gaseous and twelve condensed species were involved in the calculations. The expression adopted for the free energy of formation as a function of temperature $T$ for each compound is

$$\Delta G^\circ_f(T) = a_1 + a_2T + a_3T\ln T + a_4T^2 + a_5T^3 + a_6T^{-1} + a_7T^4 + a_8T^5 + a_9T^7 + a_{10}T^{-9} + a_{11}\ln T + a_{12}T^{-2} + a_{13}T^{-3} \quad (2)$$

The species involved are listed in Table I together with the origin of the thermodynamic values adopted. Data were mainly drawn from the Scientific Group Thermodata Europe (SGTE) databank [20] and from Barin's compilation [21]. Data on $Si_xC_y$ species were drawn from Gurvich *et al.* [22]. Because of the high temperatures considered, no liquid compounds ($H_2O$, $H_2O_2$ and organic $C_xH_yO_z$) were considered in the

TABLE I Species considered in the thermodynamic calculations and the origin of their thermodynamic description

| No. | Species | Ref. | No. | Species | Ref. |
|---|---|---|---|---|---|
| 1 | C-diamond | 23 | 27 | $C_2H_4$-gas | 20 |
| 2 | C-graphite | 23 | 28 | $C_2H_4O$-gas | 20 |
| 3 | Si-diamond | 23 | 29 | $C_2H_4O_2$-gas | 20 |
| 4 | Si-liquid | 23 | 30 | $C_2H_6$-gas | 20 |
| 5 | SiC-hexagonal, liquid | 22 | 31 | $C_2H_6O$-gas | 20 |
| 6 | SiC-cubic | 22 | 32 | $C_3$-gas | 21 |
| 7 | $SiO_2$-Lquartz | 20 | 33 | H-gas | 21 |
| 8 | $SiO_2$-Hquartz | 20 | 34 | HO-gas | 20 |
| 9 | $SiO_2$-tridymite | 20 | 35 | $HO_2$-gas | 20 |
| 10 | $SiO_2$-cristobalite | 20 | 36 | $H_2$-gas | 23 |
| 11 | $SiO_2$-liquid | 20 | 37 | $H_2O$-gas | 20 |
| 12 | $Si_2H_6$-solid | 20 | 38 | $H_2O_2$-gas | 20 |
| 13 | C-gas | 21 | 39 | O-gas | 21 |
| 14 | CH-gas | 20 | 40 | $O_2$-gas | 23 |
| 15 | CHO-gas | 20 | 41 | $O_3$-gas | 21 |
| 16 | $CH_2$-gas | 20 | 42 | Si-gas | 21 |
| 17 | $CH_2O$-gas | 20 | 43 | SiC-gas | 22 |
| 18 | $CH_2O_2$-gas | 20 | 44 | SiH-gas | 20 |
| 19 | $CH_3$-gas | 20 | 45 | SiO-gas | 21 |
| 20 | $CH_4$-gas | 20 | 46 | $SiC_2$-gas | 22 |
| 21 | $CH_4O$-gas | 21 | 47 | $SiH_4$-gas | 20 |
| 22 | CO-gas | 21 | 48 | $SiO_2$-gas | 22 |
| 23 | $CO_2$-gas | 21 | 49 | $Si_2$-gas | 21 |
| 24 | $C_2$-gas | 21 | 50 | $Si_2C$-gas | 22 |
| 25 | $C_2H$-gas | 20 | 51 | $Si_2H_6$-gas | 20 |
| 26 | $C_2H_2$-gas | 20 | 52 | $Si_3$-gas | 21 |
| | | | 53 | Ar-gas | 23 |

calculations. The gas phase was assumed to be ideal. The data for each phase of each chemical element considered (Si, C, O, H) were incorporated in the calculations of $G\text{-}H_{ser}$ as a function of temperature, equivalent to Equation 2. $G\text{-}H_{ser}$ is the Gibbs energy relative to the enthalpy of the "standard element reference", i.e. the reference phase of the element at 298.15 K. The data adopted for this function are from Dinsdale's compilation [23].

There are no thermodynamic data for amorphous $SiC_xO_y$ solid solutions, although there is strong evidence in the literature for the existence of such species (an oxycarbide network structure with carbon atoms occupying oxygen sites [24]) in ceramic fibres [1, 4, 5, 25], as well as at the SiC–$SiO_2$ interface of oxidized silicon carbide [26–28], or in the fibrous product obtained by condensation of gaseous species SiO(g) and CO(g) at 1200–1400 °C [29]. The thermochemical properties of silicon carbide fibres [12] and of silicon oxycarbide black glass [30] were studied by multiple Knudsen cell mass spectrometry, both by comparison with SiC + $SiO_2$ + C mixed powder. The measured pressures of the main gaseous species SiO and CO were observed to be much lower for each sample than the calculated equilibrium pressures. Moreover, although the measured pressures of SiO and CO gaseous species were slightly higher above the black glass and the SiC fibre, the experimental behaviour was similar to that of the SiC + $SiO_2$ + C mixed powder. Therefore the $SiC_xO_y$ solid solution can be considered as a mixture of SiC + $SiO_2$ + C in the simulation. This assumption does not allow simulation of the overall changes of the fibre during the transition period of degradation. Nevertheless, it is expected to have little influence on the calculated degradation temperature and on the fibre and gas phase composition above it, since there is no continuum left at the end of the degradation process.

In order to differentiate the chemical environments in the core and at the skin of the fibre, the quantity of Ar considered in the calculations was changed. Indeed, the volume of micropores which can exist in the core of the as-received material or can be created after the first heat treatments and, consequently, the quantity of Ar which is in contact with the condensed matter, is much less important than at the surface of the fibre. The constant $k_p$ for the chemical equilibrium between condensed and gaseous species can be written in both cases as

$$k_p = \left(\frac{\prod_{\text{pr, condensed}} \alpha_i^{n\,i}}{\prod_{\text{r, condensed}} \alpha_k^{n\,k}}\right)\left(\frac{\prod_{\text{pr, gas}} P_j^{n\,j}}{\prod_{r,gas} P_l^{n\,l}}\right) \quad (3)$$

where $\alpha$, $p$ and $n$ are the activity, partial pressure and number of moles, respectively. The subscripts r and pr refer to the reactants and the products respectively. Since there are no solution phases considered in the calculation. $\alpha_{r,\,cond} = \alpha_{pr,\,cond} = 1$. The partial pressure for each gaseous species can be written

$$p = p_{tot}\frac{n}{\sum n_{gas}} = p_{tot}\frac{n}{n_{Ar} + \sum_{pr,\,gas} n_j + \sum_{r,\,gas} n_l}$$

where $P_{tot}$ is the total pressure. Following these assumptions, Equation 3 becomes

$$k_p = \left(\frac{P_{tot}}{n_{Ar} + \sum_{pr,\,gas} n_j + \sum_{r,\,gas} n_l}\right)^{\Sigma n_j - \Sigma n_l}\left(\frac{\prod_{pr,\,gas} n_j^{n\,j}}{\prod_{r,\,gas} n_l^{n\,l}}\right) \quad (4)$$

Since $K_p$ is constant for a given temperature, it must have the same value when the same condensed species are present for two different values of $n_{Ar}$. In order to satisfy this condition the system $(n_j, n_l)$ must take two different sets of values, so the difference in the amounts of Ar in the vicinity of the condensed matter in the core and at the skin of the fibre is expected to influence the chemical equilibrium in each case. Based on the above, a very low ($10^{-4}$ g-atom) and a comparable (1 g-atom) quantity of Ar were considered in the calculations together with the 1 g-atom of reactants in order to simulate the core and the skin environments of the fibre.

## 3. Calculations

Calculations were performed for simulation of the two extreme steps of the degradation of the fibre, as defined by Le Coustumer *et al.* [1]. In each case three compositions were considered corresponding to the continuum, the continuum plus the free carbon network, and the whole fibre. The amount of the reactants was always normalized to 1 g-atom. Table II summarizes the quantities of Si, C, O, H and Ar used in each calculation.

### 3.1. Hydrogen release

The evolution of hydrogen-containing gaseous species with temperature is presented in Fig. 1, for the continuum plus carbon network part (Fig. 1a) and for the entire fibre (Fig. 1b). It appears that in both cases and for the temperatures investigated, the total amount of the available hydrogen is found in the gas phase. $H_2$ is the most important hydrogen-containing species produced, especially above 1000 K, in agreement with mass spectrometric investigations [1, 12]. Methane is also expected to be produced, but at three to four

TABLE II Quantities (g-atom) of reactants normalized to unity and of Ar, used in the different kinds of calculation; the first and second numbers in each pair (except for Ar) correspond to calculations where hydrogen was considered and not considered, respectively, while the first and second numbers in the Ar column correspond to calculations simulating the behaviour in the core and at the skin of the fibre, respectively

| Material | Quantity (g-atom) | | | | |
|---|---|---|---|---|---|
| | Si | C | O | H | Ar |
| Fibre | 0.379/ 0.392 | 0.436/ 0.451 | 0.148/ 0.157 | 0.037/ 0 | $10^{-4}$, 1 |
| Continuum + C | 0.258/ 0.278 | 0.372/ 0.403 | 0.297/ 0.319 | 0.073/ 0 | $10^{-4}$, 1 |
| Continuum | –/0.333 | –/0.283 | –/0.383 | –/0 | $10^{-4}$, 1 |

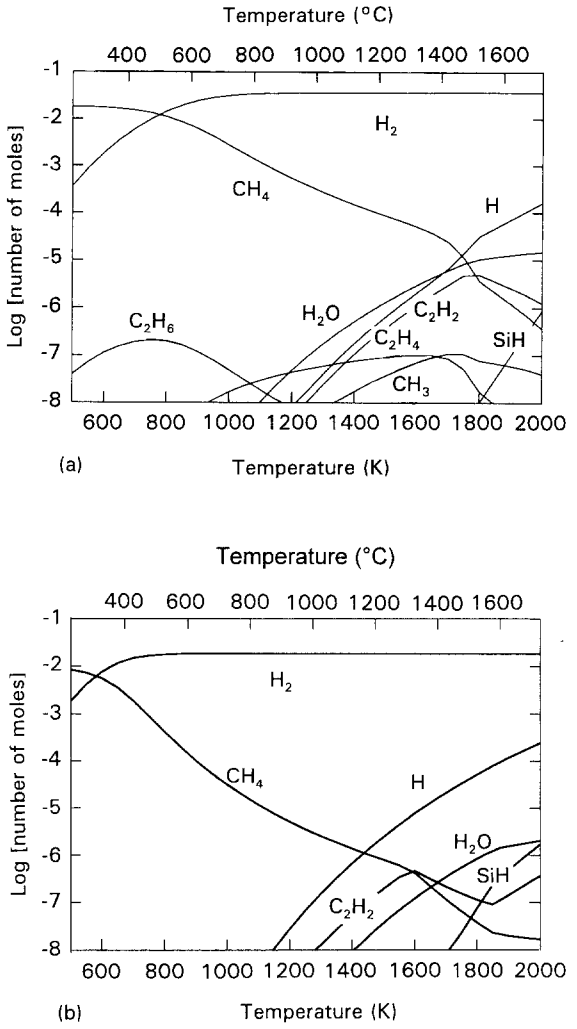


*Figure 1* Calculated hydrogen loss of the fibre, showing hydrogen-containing gaseous by-products as a function of temperature: (a) decomposition of the continuum plus free carbon parts in contact with $10^{-4}$ mol Ar, (b) decomposition of the entire fibre in contact with 1 mol Ar.

orders of magnitude less than hydrogen at 1523 K which is the reported maximum temperature for dehydrogenation of the fibre. Other species, especially H, $H_2O$ and $C_2H_2$, are produced at high temperatures but still in very low quantities compared to $H_2$. The quantities of the other-than-$H_2$ species for a given temperature are more important in Fig. 1a because of the lower ratio of the initial hydrogen to the oxygen and free carbon in the reactants.

From the complete departure of hydrogen in the gas phase at any temperature and from the continuous shape of the curves of gaseous species in Fig. 1, it appears that the results obtained do not reproduce the release of hydrogen from the free carbon network as previously reported [1]. This conclusion is compatible with TEM observations indicating that the release of hydrogen is more the result of an evolution of the organization of carbon, with an edge-to-edge association of individual and random basic structural units (BSUs) [31], performed on the depends of the C–H bonds, rather than the consequence of an abrupt modification of the chemical equilibrium at the corresponding temperature.

## 3.2. Fibre degradation

Hydrogen-containing species were not considered in the following calculations, since as previously reported [1, 12] there is almost no hydrogen left at the beginning of the main degradation step of the fibre.

Fig. 2 present the evolution with temperature of the fibre in contact with 1 mol Ar, for the condensed species (Fig. 2a) and for the gaseous species (Fig. 2b). From Fig. 2a it appears that the fibre remains stable up to 1400 K. Above this temperature the carbon content decreases slowly. At 1580 K there is an abrupt change in composition: free carbon is totally consumed, while there is a considerable increase in SiC. This event corresponds to the final step of the thermal degradation of the fibre, which was observed to occur at 1773 K.

The evolution of $SiO_2$ follows qualitatively that of carbon until 1600 K, where it reaches a new plateau for approximately 200 K. Then, at 1800 K $SiO_2$ is also totally consumed. It is, however, rather difficult to deduce from this sequence, in this as well as in the following cases, the existence and the behaviour of $SiO_2$. This species behaves as an "oxygen container" and, together with part of SiC and C it replaces in calculations the experimentally determined $SiO_xC_y$

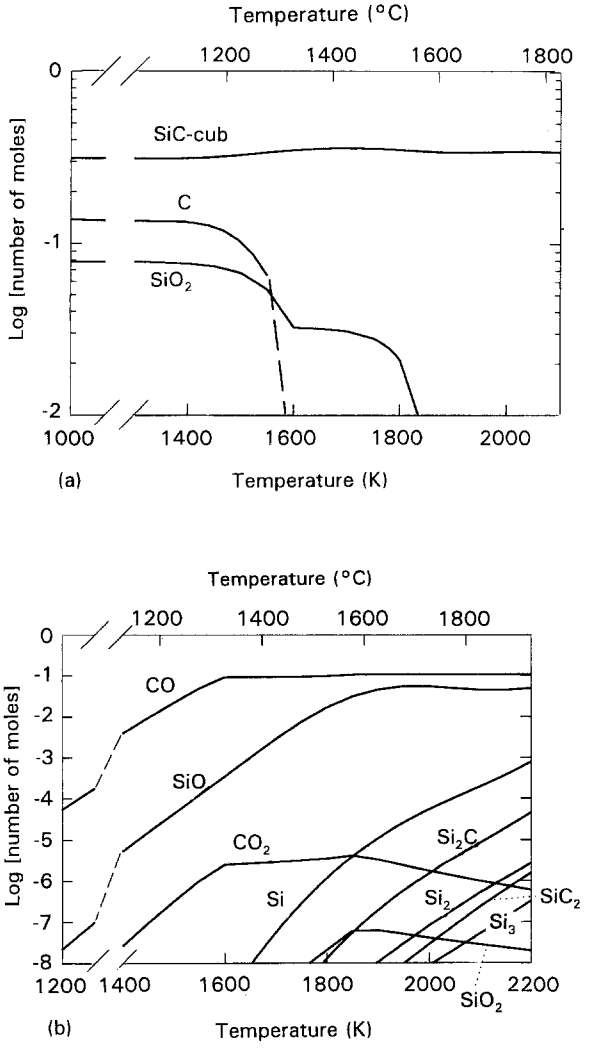


*Figure 2* Thermal evolution of the fibre, showing (a) condensed and (b) gaseous by-products in contact with 1 mol Ar as a function of treatment temperature.

solid solution. Consequently, its presence and evolution with temperature is simply representative of the quantity of oxygen available within the fibre. The decrease of $SiO_2$ at 1600 K indicates oxygen release, while the final composition of the fibre is represented by the calculated results above 1800 K.

From Fig. 2b it appears that CO is the main gas product below 1600 K. SiO and very little $CO_2$ also exist, the three of them increasing with temperature. Their evolution follows that of the condensed species. Indeed, at 1600 K, due to the complete consumption of free carbon, the increase of CO and $CO_2$ is stopped, while SiO is not affected up to 1800 K where, due to complete consumption of the condensed oxygen-containing species, it reaches a plateau. Silicon-containing gaseous species with Si predominant appear at higher temperatures in relatively low quantities.

Fig. 3 shows the evolution of the condensed species with temperature in the same conditions as in Fig. 2, for an initial composition corresponding to the continuum alone. Again at about 1600 K the available "free" carbon is totally consumed while SiC increases. The oxygen content decreases and it finally becomes nil at higher temperature. From a comparison of Figs 2a and 3 and from the evolution of the gas phase which is, in this case, qualitatively the same as in Fig. 2b, it appears that the behaviour of the fibre above presented is due to evolution of the continuum.

Fig. 4 presents the evolution with temperature of the fibre in contact with $10^{-4}$ mol Ar, for the condensed species (Fig. 4a) and for the gaseous species (Fig. 4b). The general shapes of the two figures are equivalent to Fig. 2a and b, respectively, with two main differences: the shape of the curves is now flatter and more abrupt, and the degradation temperature is shifted to 1785 K, to be compared to the experimentally determined upper limit of the degradation temperature of 1773 K.

Fig. 5 shows the evolution of the condensed species with temperature, under the same conditions as in Fig. 4, for an initial composition corresponding to the continuum alone. Once more the curves are flatter and changes are more abrupt than in Fig. 3. From the comparison of Figs 5 and 4a it clearly appears that the behaviour of the whole fibre is controlled by degradation of the continuum itself.

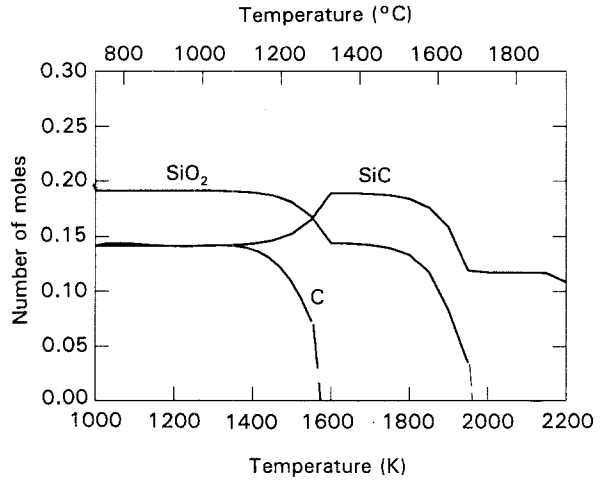


*Figure 3* Thermal evolution of the continuum part of the fibre, showing condensed products in contact with 1 mol Ar as a function of treatment temperature.

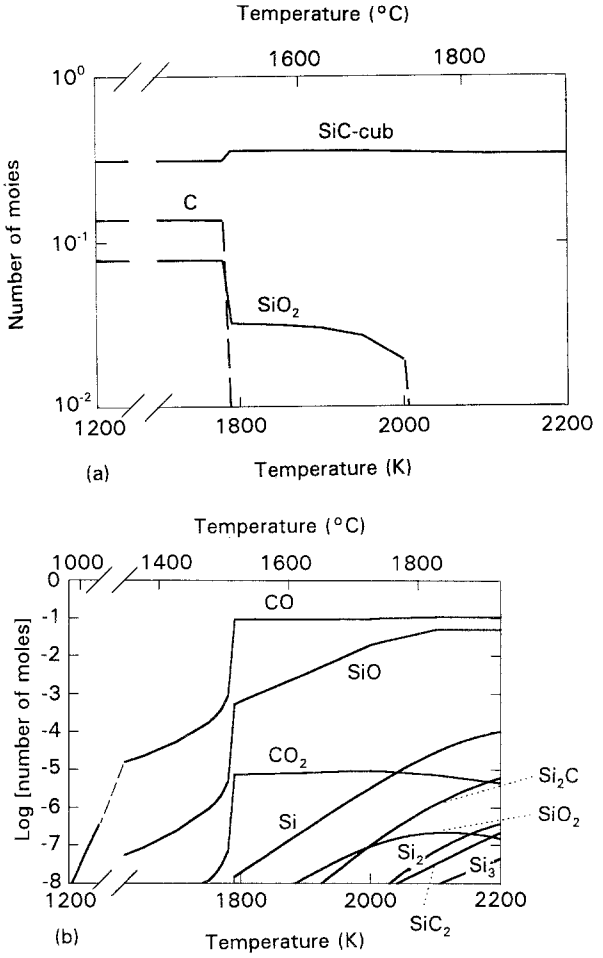


*Figure 4* Thermal evolution of the fibre, showing (a) condensed and (b) gaseous by-products in contact with $10^{-4}$ mol Ar as a function of treatment temperature.

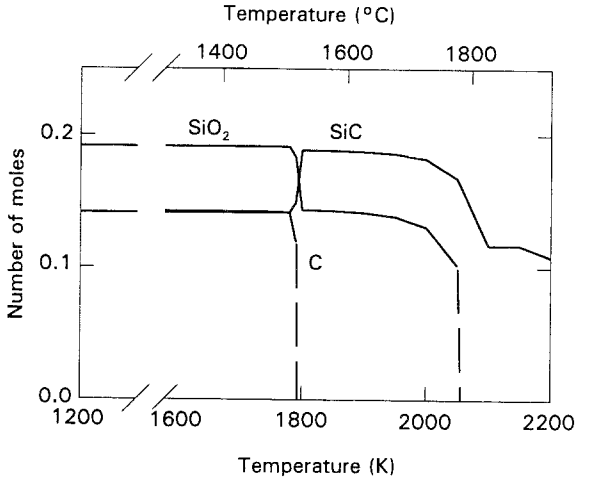


*Figure 5* Thermal evolution of the continuum part of the fibre, showing condensed products in contact with $10^{-4}$ mol Ar as a function of treatment temperature.

## 3.3. Which quantity of Ar is closer to the experimental conditions?

The calculated transition in the composition of the condensed and gaseous species as a function of tem-

perature illustrates the thermal degradation of the fibre. However, the temperature which corresponds to this phenomenon depends on the dilution of the reactants, i.e. the Ar flow or the available volume above the fibre: it increases from 1580 K for 1 g-atom Ar per g-atom to 1785 K for $10^{-4}$ g-atom Ar per g-atom. In order to verify if the above selected dilutions and, consequently, the corresponding degradation temperatures, are single points, i.e. if they are characteristic of a particular situation concerning the thermal treatment of the material, the relationship between these two parameters is established and illustrated in Fig. 6. It appears that the degradation temperature does not depend on the dilution of the reactants up to approximately $10^{-2}$ g-atom Ar per g-atom. For higher dilution it decreases linearly with the logarithm of the quantity of Ar.

Following this diagram and for a given total pressure, there is a limit value above which the higher the inert gas flow or the higher the available volume above the fibre, the lower the temperature where the final step of its thermal degradation occurs. Calculations made with 1 g-atom Ar per g-atom lead to results which have no general value and, since it is not possible to establish precisely the quantity of Ar in contact with the fibre, they also may not correspond to the experimental conditions at the skin of the fibre. A way to resolve this problem would be to determine by mass spectrometric measurements the production rate of, for example, CO in the experimental conditions studied, and then calculate the quantity of Ar which yields the same quantity of CO in the thermodynamic simulation. However, attention must be paid in this kind of experiment to the important kinetic limitations, extensively developed in earlier work [12, 19, 30].

In contrast to the previous remarks, it appears from Fig. 6 that calculations made with $10^{-4}$ g-atom Ar per g-atom are situated in a domain where chemical equilibrium does not depend on dilution of the gas phase. They have a more general value and can represent the situation in the core of the fibre. Since in the intermediate degradation step reported by Le Coustumer *et al.* [1] the skin thickness represents 1/30th of the mean radius of the fibre, it can be admitted that the major part of the material is found in a "core" environment and that the calculations made with $10^{-4}$ g-atom Ar represent better its global behaviour. This suggestion is supported by the close fit for the degradation temperature between the calculated value (1785 K) and the experimentally determined value of 1773 K. Additionally, the calculated CO partial pressure above the degradation temperature is almost equal to 1 atm, in agreement with the *a priori* assumption of Yamaguchi [13] on the atmosphere within a Si, C and O containing refractory. Indeed, the $SiO_2$–SiC–C equilibrium point for $P_{CO} = 1$ atm was calculated by Yamaguchi [13] and also by Gulbransen and Jansson [14] to be at 1800 K.

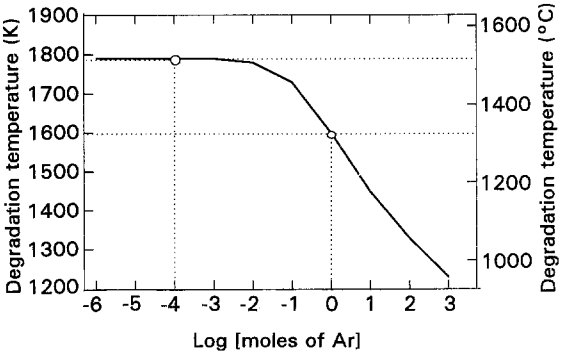


*Figure 6* Thermal evolution of the fibre, showing degradation temperature as a function of the number of moles of Ar available. Dotted lines correspond to the conditions investigated.

## 3.4 Weight loss and oxygen content

Fig. 7 presents the weight loss of the fibre as determined thermogravimetrically, compared with thermodynamic calculations made with $10^{-4}$ g-atom Ar per g-atom. Both curves present a marked weight loss in the same temperature range of 1700–1850 K, in

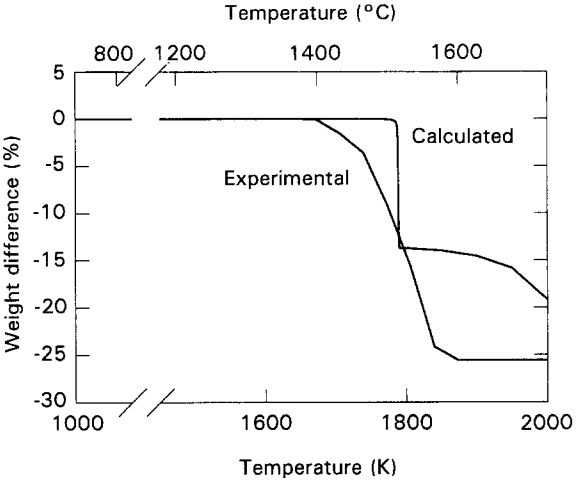


*Figure 7* Thermal evolution of the fibre, showing weight loss as a function of treatment temperature. Calculated (for $10^{-4}$ mol Ar) and experimental thermogravimetric curves.

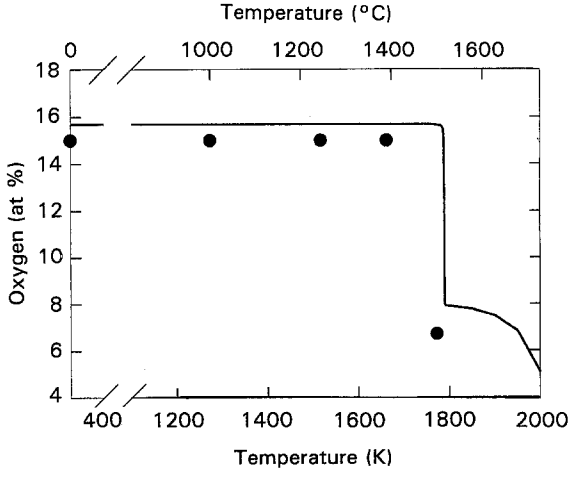


*Figure 8* Oxygen content of the fibre as a function of treatment temperature: (●) experimental [1] and (——) calculated results.

agreement with the determined degradation temperature. The experimentally determined slope is smoother than the calculated one. The experimentally determined weight loss begins about 70 K earlier and it reaches a final value of 25%, 10% more than the calculated value. This misfit can support the previously mentioned suggestion that a minor part of the fibre, i.e. its external envelope, is exposed to more severe degradation conditions than the conditions adopted for calculation of the theoretical thermogravimetric curve.

Fig. 8 presents the oxygen content of the fibre as a function of treatment temperature. The points are experimental results from Le Coustumer *et al.* [1] and are compared with the calculated results of this work. Although there is a systematic misfit of about 1%, the agreement between the two sets of results is excellent.

### 3.5. Reaction mechanisms

The predominant reaction in the temperature range where condensed C, $SiO_2$ and SiC coexist is

$$3C_{(s)} + SiO_{2(s)} \rightleftharpoons SiC_{(s)} + 2CO_{(g)} \quad (5)$$

Reaction 5 fits well the evolution of the quantities of the condensed phases relative to each other. Indeed, under the same conditions as in Fig. 4, at the temperature of total free carbon consumption (1785 K), Reaction 5 leads to 0.0327 g-atom $SiO_2$ and 0.3593 g-atom SiC. These quantities as well as the resulting weight loss are identical within 0.1% with the corresponding calculated values.

In the temperature range between consumption of the free carbon and that of $SiO_2$, the reaction which best fits the calculated results is

$$SiC_{(s)} + 2SiO_{2(s)} \rightleftharpoons 3SiO_{(g)} + CO_{(g)} \quad (6)$$

The calculated results confirm the proposed global endogenous oxidation mechanism which is represented by Equation 1. Indeed, the ratio of CO to SiO in Equation 1 is 2.3 compared to 2.2 in Fig. 4b at high temperatures, i.e. when all the oxygen available is completely consumed. At lower temperatures, i.e. when there is still oxygen left in the condensed phases, this ratio is calculated to be two orders of magnitude higher. This result is in disagreement with mass spectrometric measurements of CO and SiO above the fibre [12], showing at the same range of temperature a CO/SiO ratio slightly higher than unity. The misfit can be due to control of the degradation by kinetic factors as already developed [12], but additionally to the assumption made in calculations of completely crystallized condensed phases. This point was discussed by Luthra [16], who considered the amorphous state as a supercooled liquid and calculated the activities of the constituents from the estimated temperatures and entropies of melting and from the activities in the solid state. The gas phase composition obtained has a lower CO content relative to SiO, compared to calculations where the activities of the condensed species were considered equal to unity.

## 4. Conclusions

The thermal degradation of the Nicalon fibre NLM-202 was theoretically investigated by performing thermochemical calculations in the Si–C–O–H chemical system and was compared with recently published experimental results. The environments in the core and at the skin of the fibre were differentiated by adopting different inert gas dilutions of the reactants. It was confirmed that the hydrogen loss characterizing the first degradation step is due to rearrangement of the free carbon network rather than to chemical events. The main step of the observed degradation mechanism was successfully simulated in terms of the temperature, oxygen content and weight loss of the material. The proposed endogenous oxidation mechanism of the fibre was globally verified.

The coherence between the calculated and experimental results indicates that thermodynamic simulation can be used as a basis for modelling the thermal and/or chemical behaviour of ceramic materials at elevated temperatures. The elaboration of complete and accurate thermodynamic data is necessary for the improvement of this approach. However, the simultaneous consideration of appropriate kinetic and diffusional parameters is often necessary in order to improve the reliability of the model and to allow, when associated with nanotexture characterization, for an understanding of the reaction mechanisms and finally for the manufacture of materials with predictable properties.

## Acknowledgements

Thanks are due to Philippe Le Coustumer and to Marc Monthioux (CNRS, Pau) for fruitful discussions and to Pierre-Yves Chevalier and to Evelyne Fischer (Thermodata, Grenoble) for help with the GEMINI2 software.

## References

1. P. Le COUSTUMER, M. MONTHIOUX and A. OBERLIN, *J. Eur. Ceram. Soc.* **11** (1993) 95.
2. P. SCHRECK, C. VIX-GUTERL, P. EHRBURGER and J. LAHAYE, *J. Mater. Sci.* **27** (1992) 4237.
3. *Idem, ibid.* **27** (1992) 4243.
4. L. PORTE and A. SARTRE, *ibid* **24** (1989) 271.
5. C. LAFFON, A. M. FLANK, P. LAGARDE, M. LARIDJANI, R. HAGEGE, P. OLRY, J. COTTERET, J. DIXMIER, J. L. MIQUEL, H. HOMMEL and A. P. LEGRAND, *ibid* **24** (1989) 1503.
6. T. MAH, N. L. HECHT, D. E. McCULLUM, J. R. HOENIGMAN, H. M. KIM, A. P. KATZ and H. A. LIPSITT, *ibid*, **19** (1984) 1191.
7. T. J. CLARK, R. M. ARONS and J. B. STAMATOFF, *Ceram. Eng. Sci. Proc.* **6** (1985) 576.
8. S. M. JOHNSON, R. D. BRITTAIN, R. H. LAMOREAUX and D. J. ROWCLIFFE, *J. Amer. Ceram. Soc.* **71** (1988) C132.
9. T. SHIMOO, M. SUGIMOTO and K. OKAMURA, *Nippon Seramikkusu kyokai Gakujutsu Rombunshi* (*J. Ceram. Soc. Jpn*) **98** (1990) 1324.
10. *Idem, J. Jpn Inst. Met.* **54** (1990) 802.
11. T. SHIMOO, H. CHEN and K. OKAMURA, *J. Ceram. Soc. Jpn* **100** (1992) 48.
12. P. ROCABOIS, C. CHATILLON and C. BERNARD, in Proceedings of Conference on High Temperature Ceramic

Matrix Composites–ECCM6, Bordeaux, September 1993, edited by R. Naslain, J. Lamon and D. Doumeingts, (Woodhead Publ., Cambridge, 1993) p. 20.
13. A. YAMAGUCHI, *Taikabutsu Overseas* **4**(3) (1984) 14.
14. E. A. GULBRANSEN and S. A. JANSSON, *Oxid. Met.* **4**(3) (1972) 181
15. S. C. SINGHAL, *Ceramurgia Int.* **2**(3) (1976) 123.
16. K. L. LUTHRA, *J. Amer. Ceram. Soc.* **69** (1986) C-231.
17. P. GREIL, *J. Eur. Ceram. Soc.* **6** (1990) 53.
18. P. M. BENSON, K. E. SPEAR and C. G. PANTANO, in "Ceramic Microstructures '86", edited by Pask and Evans (Plenum, 1988) pp. 415–425.
19. N. S. JACOBSON, K. N. LEE and D. S. FOX, *J. Amer. Ceram. Soc.* **75** (1992) 1603.
20. Scientific Group Thermodata Europe, available on line from Thermodata, BP66 F-38402 Saint Martin d'Hères, France and Royal Institute of Technology, S-10044 Stockholm, Sweden.
21. I. BARIN (ed.), in "Thermochemical Data of Pure Substances" (VCH, Weinheim, Germany, 1989) pp. 212, 213, 262, 1092, 1094, 1335–1337, 1358.
22. L. V. GURVICH, I. V. VEYTS and C. B. ALCOCK, in "Thermodynamic Properties of Individual Substances", 4th Edn, Vols 1 and 2, edited by L. V. Gurvich, I. V. Veyts and C. B. Alcock (Hemisphere, New York, 1990) pp. 233, 262, 263, 265–267.
23. A. T. DINSDALE, in "SGTE Data for Pure Elements", NPL report DMA(A) 195 (National Physical Laboratory, Teddington, 1989).
24. H. ZHANG and C. G. PANTANO, *J. Amer. Ceram. Soc.* **74** (1990) 958.
25. J. LIPOWITZ, H. A. FREEMAN, R. T. CHEN and E. R. PRACK, *Adv. Ceram. Mater.* **2** (1987) 121.
26. R. PAMPOUCH, W. S. PTAK, S. JONAS and J. STOCH, in Proceedings of the 9th International Symposium on Reactivity of Solids, edited by K. Direk, J. Habber and J. Novotng (1980) pp. 674–684.
27. B. O. YAVUZ and L. L. HENCH, *Ceram. Eng. Sci. Proc.* **3** (1982) 596.
28. R. BERJOAN, J. RODRIGUEZ and F. SIBIEUDE, *Surf. Sci* **271** (1992) 237.
29. A. JULBE, A. LARBOT, C. GUIZARD and L. COT, *Eur. J. Solid State Inorg. Chem.* **26** (1989) 101.
30. P. ROCABOIS, C. CHATILLON and C. BERNARD, *Surf. Coatings Technol.* **61** (1993) 86.
31. A. OBERLIN, in "Chemistry and Physics of Carbon", edited by P. A. Thrower (Dekker, New York, 1989) p. 1.

*Received 9 November 1993*
*and accepted 28 April 1994*